10930 Inorg. Chem. 2010, 49, 10930–10939
DOI: 10.1021/ic101271d

Inorganic Chemistry
Article

Computational Studies on the Photophysical Properties and NMR Fluxionality of Dinuclear Platinum(II) A-Frame Alkynyl Diphosphine Complexes

Wai Han Lam* and Vivian Wing-Wah Yam*

Institute of Molecular Functional Materials and Department of Chemistry, The University of Hong Kong, Pokfulam Road, Hong Kong, People's Republic of China

Received June 26, 2010

The structural geometry, electronic structure, photophysical properties, and the fluxional behavior of a series of A-frame diplatinum alkynyl complexes, $[Pt_2(\mu\text{-dppm})_2(\mu\text{-C}{\equiv}\text{CR})(\text{C}{\equiv}\text{CR})_2]^+$ [R = ^{t}Bu (**1**), C_6H_5 (**2**), C_6H_4Ph-*p* (**3**), C_6H_4Et-*p* (**4**), C_6H_4OMe-*p* (**5**); dppm = bis(diphenylphosphino)methane], have been studied by density functional theory (DFT) and time-dependent TD-DFT associated with conductor-like polarizable continuum model (CPCM) calculations. The results show that the Pt···Pt distance strongly depends on the binding mode of the alkynyl ligands. A significantly shorter Pt···Pt distance is found in the symmetrical form, in which the bridging alkynyl ligand is σ-bound to the two metal centers, than in the unsymmetrical form where the alkynyl ligand is σ-bound to one metal and π-bound to another. For the two structural forms in **1**−**5**, both the highest occupied molecular orbital (HOMO) and the lowest unoccupied molecular orbital (LUMO) energy levels show a dependence on the nature of the substituents attached to the alkynyl ligand. The energies of the HOMO and LUMO are found to increase and decrease, respectively, from R = ^{t}Bu to R = Ph and to R = C_6H_4Ph-*p*, because of the increase of the π- conjugation of the alkynyl ligand. On the basis of the TDDFT/CPCM calculations, the low-energy absorption band consists of two types of transitions, which are ligand-to-ligand charge-transfer (LLCT) [π(alkynyl) → σ*(dppm)]/metal-centered MC [dσ*(Pt_2) → pσ(Pt_2)] transitions as well as interligand $\pi \rightarrow \pi^*$ transition from the terminal alkynyl ligands to the bridging alkynyl ligand mixed with metal-metal-to-ligand charge transfer MMLCT [dσ*(Pt_2) → π*(bridging alkynyl)] transition. The latter transition is lower in energy than the former. The calculation also indicates that the emission for the complexes originates from the triplet interligand π(terminal alkynyls) → π*(bridging alkynyl)/MMLCT [dσ*(Pt_2) → π*(bridging alkynyl)] excited state. In terms of the fluxional behavior, calculations have been performed to study the details of the mechanisms for the three fluxional processes, which are the σ,π-alkynyl exchange, the ring-flipping, and the bridging-to-terminal alkynyl exchange processes.

Introduction

The first dinuclear metal complexes having the A-frame geometry were reported in 1977.[1] Since that time, numerous other reports of A-frame complexes and their reaction chemistry have appeared.[2−7] The idealized A-frame structure has each metal center being square planar and tied together through a common ligand at the apex of the A. The metal centers are usually Rh, Ir, Pd, and Pt and they are bridged by two bis(diphenylphosphino)methane (dppm) ligands in the *trans* arrangement with the methylene linkages of the dppm groups folded toward the apex of the A-frame. The apical ligand shows great diversity, ranging from single atom bridges such as H,[5b−d,6a−6d] S,[1a,3a−3c] and Cl[4f,6e] to small molecules such as CO,[3d−f] CH_2,[5a,e] SO_2,[4e,7c] C≡NR,[1b,7d] and C≡CR.[4a−d] If the bridging ligand is an alkynyl ligand, two bridging modes have been observed; either it can bind in

---

*To whom correspondence should be addressed. E-mail: wwyam@hku.hk, chsue@hku.hk . Fax: +(852) 2857-1586. Phone: +(852) 2859-2153.

[1] (a) Kubiak, C. P.; Eisenberg, R. *J. Am. Chem. Soc.* **1977**, *99*, 6129. (b) Olmstead, M. M.; Hope, H.; Benner, L. S.; Balch, A. L. *J. Am. Chem. Soc.* **1977**, *99*, 5502.

[2] (a) Ye, C.; Sharp, P. R. *Inorg. Chem.* **1995**, *34*, 55. (b) Ge, Y.-W.; Sharp, P. R. *Inorg. Chem.* **1993**, *32*, 94. (c) Ge, Y.-W.; Sharp, P. R. *J. Am. Chem. Soc.* **1990**, *112*, 3667. (d) Ge, Y.-W.; Peng, F.; Sharp, P. R. *J. Am. Chem. Soc.* **1990**, *112*, 2632. (e) Sharp, P. R.; Ge, Y.-W. *J. Am. Chem. Soc.* **1987**, *109*, 3796. (f) Sharp, P. R.; Flynn, J. R. *Inorg. Chem.* **1987**, *26*, 3231.

[3] (a) Oldham, S. M.; Houlis, J. F.; Sleigh, C. J.; Duckett, S. B.; Eisenberg, R. *Organometallics* **2000**, *19*, 2985. (b) Kubiak, C. P.; Woodcock, C.; Eisenberg, R. *Inorg. Chem.* **1980**, *19*, 2733. (c) Kubiak, C. P.; Eisenberg, R. *Inorg. Chem.* **1980**, *19*, 2726. (d) Anderson, D. J.; Kramarz, K. W.; Eisenberg, R. *Inorg. Chem.* **1996**, *35*, 2688. (e) Kramarz, K. W.; Eisenberg, R. *Organometallics* **1992**, *11*, 1997. (f) Kramarz, K. W.; Eisenschmid, T. C.; Deutsch, D. A.; Eisenberg, R. *J. Am. Chem. Soc.* **1991**, *113*, 5090. (g) Woodcock, C.; Eisenberg, R. *Organometallics* **1985**, *4*, 4.

[4] (a) George, D. S. A.; Hilts, R. W.; McDonald, R.; Cowie, M. *Organometallics* **1999**, *18*, 5330. (b) George, D. S. A.; McDonald, R.; Cowie, M. *Organometallics* **1998**, *17*, 2553. (c) Cowie, M.; Loeb, S. J. *Organometallics* **1985**, *4*, 852. (d) Deraniyagala, S. P.; Grundy, K. R. *Organometallics* **1985**, *4*, 424. (e) Cowie, M.; Dwight, S. K. *Inorg. Chem.* **1980**, *19*, 209. (f) Cowie, M.; Dwight, S. K. *Inorg. Chem.* **1979**, *18*, 2700.

Scheme 1. (a) Symmetrical and (b) Unsymmetrical Forms

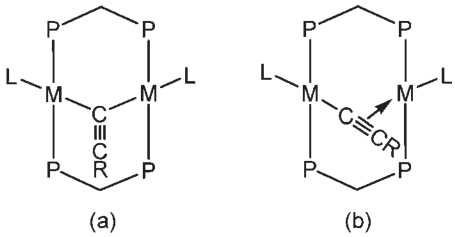

Scheme 2. Complexes **1**−**6**

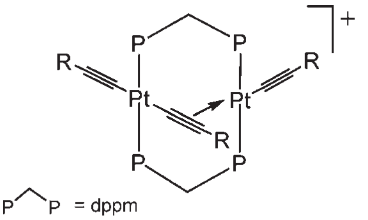

R = ^{t}Bu (**1**)
= C_6H_5 (**2**)
= C_6H_4Ph-*p* (**3**)
= C_6H_4Et-*p* (**4**)
= C_6H_4OMe-*p* (**5**)
= C_6H_4OEt-*p* (**6**)

a symmetrical manner, σ-bound to the two metal centers (symmetrical form), or it can bind unsymmetrically, σ-bound to one metal and π-bound to another (unsymmetrical form), as shown in Scheme 1a and 1b, respectively.

In 1980, Shaw et al. reported the first A-frame platinum alkynyl complex, $[Pt_2(\mu\text{-dppm})_2(\mu\text{-C}\equiv\text{C}^t\text{Bu})(\text{C}\equiv\text{C}^t\text{Bu})_2]^+$ with all three alkynyl ligands in the equatorial position.[8] The photophysical properties were not reported until 1993 when Yam and co-workers performed a systematic study of the excited state chemistry on a series of A-frame dinuclear platinum alkynyl complexes, $[Pt_2(\mu\text{-dppm})_2(\mu\text{-C}\equiv\text{CR})(\text{C}\equiv\text{CR})_2]^+$ **1**−**6** (Scheme 2).[9] It was reported that the A-frame platinum(II) alkynyl complexes possess long-lived excited states and are strongly emissive both in the solid state and in fluid solution. The lowest energy absorption and emission bands of all the A-frame alkynyl complexes are found to be red-shifted with respect to the related mononuclear species, *trans*-$[Pt(\text{dppm-P})_2(\text{C}\equiv\text{CR})_2]$. In addition, the energies are found to show a blue shift on going from the aryl-substituted alkynyl complexes **2**−**6** to the alkyl-substituted alkynyl complex **1**. On the basis of the observed trends, the lowest energy absorption band was assigned as a metal-metal-to-ligand charge transfer (MMLCT) $[d\sigma^*(Pt_2) \rightarrow \pi^*(\text{C}\equiv\text{CR})]$ transition mixed with a metal-centered $[d\sigma^*(Pt_2) \rightarrow p\sigma(Pt_2)]$ transition, and the emission band was likely derived from a triplet MMLCT/MC excited state.

Scheme 3. (a) σ,π-Alkynyl Exchange, (b) Ring-Flipping, and (c) Bridging-to-Terminal Alkynyl Exchange Processes

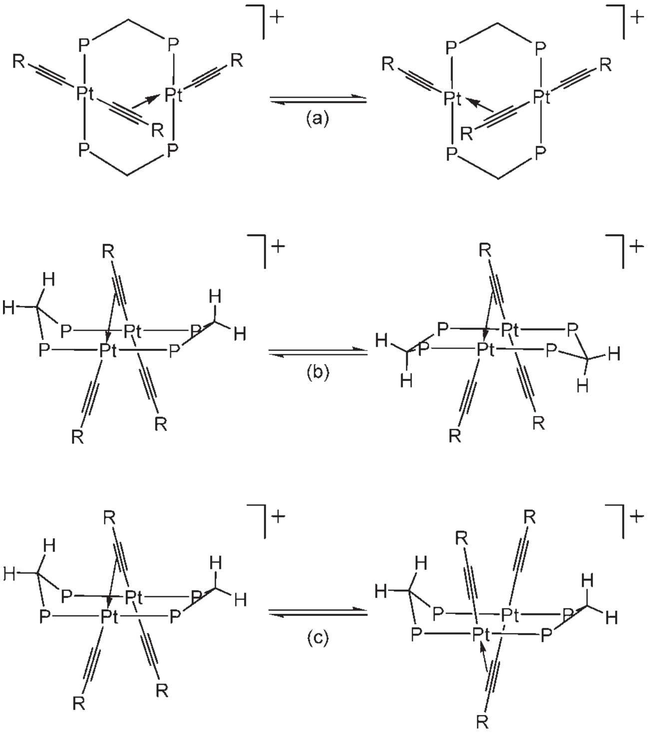

In addition to the rich luminescent properties, these A-frame alkynyl complexes have been found to exhibit interesting fluxional properties in solution.[9b,c] The room-temperature ^{1}H NMR spectra of complexes **1**−**6** all showed two broad multiplets for the two methylene protons (H_α and H_β) of the dppm ligands. It is worth mentioning that the boat structure with the two methylene groups pointing toward the apical position is commonly observed for most of the A-frame complexes. For complexes **1**, **5**, and **6**, only two sets of resonances over the temperature range from −40 °C to room temperature in a 2:1 ratio were observed for the alkynyl groups, indicating the equivalence of the two terminal alkynyl ligands. However, at temperature near 321 K, only a single broad signal was observed for the two methylene protons. For complexes **1**, **5**, and **6**, apart from the observation of the single broad methylene proton signal, only one set of the resonances for the bridging and terminal alkynyl ligands was found. The coalescence temperature for the methylene protons and alkynyl ligands in **1**, **5**, and **6** occurs in the range of 314−330 K. Similar to almost identical free energies of activation ($\Delta G^{\ddagger}$) values of 15.5 kcal mol^{-1} were found, suggesting that the rapid exchange of the methylene protons and the alkynyl ligands are related and may originate from the same fluxional process.

On the basis of the observations from the ^{1}H NMR spectroscopic results, three fluxional processes are proposed. The σ,π-alkynyl exchange, in which the bridging alkynyl group moves from metal to metal in a "windscreen-wiper" manner (Scheme 3a), renders the two terminal alkynyl ligands

---

(5) (a) Azam, K. A.; Frew, A. A.; Lloyd, B. R.; Manojlović-Muir, Lj.; Muir, K. W.; Puddephatt, R. J. *Organometallics* **1985**, *4*, 1400. (b) Azam, K. A.; Puddephatt, R. J. *Organometallics* **1983**, *2*, 1396. (c) Hill, R. H.; De Mayo, P.; Puddephatt, R. J. *Inorg. Chem.* **1982**, *10*, 3642. (d) Brown, M. P.; Cooper, S. J.; Frew, A. A.; Manojlović-Muir, Lj.; Muir, K. W.; Puddephatt, R. J.; Thomson, M. A. *J. Chem. Soc., Dalton Trans.* **1982**, 299. (e) Brown, M. P.; Fisher, J. R.; Puddephatt, R. J.; Seddon, K. R. *Inorg. Chem.* **1979**, *18*, 2808. (f) Neve, F.; Ghedini, M.; De Munno, G.; Crispini, A. *Inorg. Chem.* **1992**, *31*, 2979. (g) Neve, F.; Ghedini, M.; Tiripicchio, A.; Ugozzoli, F. *Organometallics* **1992**, *11*, 795.

(6) (a) Janka, M.; Anderson, G. K.; Rath, N. P. *Organometallics* **2000**, *19*, 5071. (b) Stockland, R. A., Jr.; Anderson, G. K.; Rath, N. P. *Inorg. Chim. Acta* **2000**, *300*−*302*, 395. (c) Xu, C.; Anderson, G. K. *Organometallics* **1996**, *15*, 1760. (d) Xu, C.; Anderson, G. K. *Organometallics* **1994**, *13*, 3981. (e) Fallis, K. A.; Xu, C.; Anderson, G. K. *Organometallics* **1993**, *12*, 2243.

(7) (a) Lee, C.-L.; Hunt, C. T.; Balch, A. L. *Organometallics* **1982**, *1*, 824. (b) Balch, A. L.; Hunt, C. T.; Lee, C.-L.; Olmstead, M. M.; Farr, J. P. *J. Am. Chem. Soc.* **1981**, *103*, 3764. (c) Balch, A. L.; Benner, L. S.; Olmstead, M. M. *Inorg. Chem.* **1979**, *18*, 2996. (d) Benner, L. S.; Balch, A. L. *J. Am. Chem. Soc.* **1978**, *100*, 6099.

(8) Langrick, C. R.; McEwan, D. M.; Pringle, P. G.; Shaw, B. L. *J. Chem. Soc., Dalton Trans.* **1983**, 2487.

(9) (a) Yam, V. W.-W.; Chan, L.-P.; Lai, T.-F. *Organometallics* **1993**, *12*, 2197. (b) Yam, V. W.-W.; Yeung, P. K.-Y.; Chan, L.-P.; Kwok, W.-M.; Phillips, D. L.; Yu, K.-L.; Wong, R. W.-K.; Yan, H.; Meng, Q.-J. *Organometallics* **1998**, *17*, 2590. (c) Wong, K. M.-C.; Hui, C.-K.; Yu, K.-L.; Yam, V. W.-W. *Coord. Chem. Rev.* **2002**, *229*, 123.

Scheme 4. Planar Structure

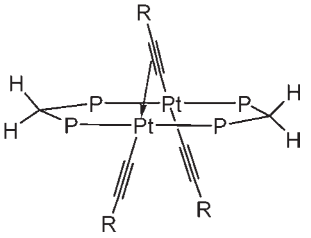

equivalent even at −40 °C. On the other hand, the concurrent equilibration of the methylene protons and the alkynyl units is likely to involve a ring flipping process (Scheme 3b) accompanied by a bridging-to-terminal alkynyl ligand exchange (Scheme 3c). As shown in Scheme 3b and 3c, both ring-flipping and bridging-to-terminal alkynyl exchange processes will result in the formation of an inverted-boat structure in which the two methylene groups are pointing away from the apical position (A-frame inversion). It was proposed that the flipping process is facile and occurs readily with a small activation energy, giving a time-averaged structure with the $Pt_2P_4C_2$ unit lying on the same plane (Scheme 4). However, the ring-flipping process alone would not be able to remove the nonequivalence of the methylene protons because of the A-frame structure. It is believed that at high temperatures, the bridging-to-terminal alkynyl exchange would occur, with interactions between the alkynyl groups and the dppm phenyl groups requiring both the ring flipping and the bridging-to-terminal alkynyl exchange processes to occur in a concerted fashion, since ring flipping would also exchange the positions of the phenyl groups. This leads to the equivalence of both the alkynyl ligands and the methylene protons. Thus the $\Delta G^{\ddagger}$ value obtained measures the rate of the bridging-to-terminal alkynyl exchange process.[9b]

In view of the interesting properties observed for the A-frame dinuclear platinum alkynyl complexes as well as the potential applications of the A-frame dinuclear complexes as photonic materials,[10] and multicentered reagents and catalysts,[11] a computational study on a series of the A-frame alkynyl complexes was pursued to investigate their structural geometry, nature of electronic absorption and emission, as well as the possible mechanisms for the fluxional processes. In terms of the structural geometry, it is interesting to note that an intramolecular Pt$\cdots$Pt distance of 3.236 Å was observed in the X-ray crystal structure of **2**, where the bridging alkynyl ligand unsymmetrically binds to the two metal centers, while a shorter Pt$\cdots$Pt distance (2.903 Å) was found for the complex $[Pt_2(\mu\text{-dppm})_2(\mu\text{-C}{\equiv}CC_6H_4{}^{n}Bu\text{-}p)(C{\equiv}CC_6H_4{}^{n}Bu\text{-}p)_2]^+$, where the bridging alkynyl ligand symmetrically binds to the two metal centers.[9c] Through this study, it is hoped that insights into the factors which govern the Pt$\cdots$Pt separations in the A-frame complexes and the effect of the substituents of the alkynyl group on the relative stability of the symmetrical and unsymmetrical forms can be obtained. In addition, the nature of the orbitals involved in the transitions for the lowest-energy absorption and emission will be discussed and correlated to the nature of the alkynyl ligands. Finally, the details of the possible mechanisms for the fluxional processes will also be described.

Computational Details

Calculations were carried out using Gaussian 03 software package.[12] Geometry optimization was performed for complexes **1**−**5** (Scheme 2) with the bridging alkynyl ligand bound in the symmetrical (**1a**−**5a**) and unsymmetrical manner (**1b**−**5b**) as well as the species involved in the fluxional processes for complexes **1** and **2** by using density functional theory (DFT) at the hybrid Perdew, Burke, and Ernzerhof functional (PBE0) level.[13] On the basis of the ground state optimized geometries of the two forms in **1**−**5** in the gas phase, the non-equilibrium time-dependent TD-DFT method[14] at the same level associated with the conductor-like polarizable continuum model (CPCM)[15] using CH_3CN as the solvent was employed to compute the low-energy singlet−singlet and singlet−triplet transitions. On the basis of the ground-state optimized structure of **2a** and **2b**, the unrestricted UPBE0 was used to optimize the first triplet excited state to determine the nature of the distortion relative to the corresponding ground state. Vibrational frequencies were calculated for all stationary points to verify that each was a minimum (NIMAG = 0) or a transition state (NIMAG = 1) on the potential energy surface and to obtain the thermal corrections needed to convert energy differences to free energy differences. For all the calculations, the Stuttgart effective core potentials (ECPs) and the associated basis sets were applied to describe Pt,[16] while the 6-31G basis set[17] was used for all other atoms. In addition, f-type polarization functions for the Pt atom ($\zeta = 0.993$),[18] and d-type polarization

---

(10) (a) Clément, S.; Aly, S. M.; Bellows, D.; Fortin, D.; Strohmann, C.; Guyard, L.; Abd-El-Aziz, A. S.; Knorr, M.; Harvey, P. D. *Inorg. Chem.* **2009**, *48*, 4118. (b) Clément, S.; Aly, S. M.; Husson, J.; Fortin, D.; Strohmann, C.; Knorr, M.; Guyard, L.; Abd-El-Aziz, A. S.; Harvey, P. D. *Eur. J. Inorg. Chem.* **2009**, 2536. (c) Clément, S.; Aly, S. M.; Fortin, D.; Guyard, L.; Knorr, M.; Abd-El-Aziz, A. S.; Harvey, P. D. *Inorg. Chem.* **2008**, *47*, 10816. (d) Clément, S.; Aly, S. M.; Gagnon, K.; Abd-El-Aziz, A. S.; Knorr, M.; Harvey, P. D. *J. Inorg. Organomet. Polym.* **2008**, *18*, 104.

(11) (a) Cowie, M. *Can. J. Chem.* **2005**, *83*, 1043. (b) Hilts, R. W.; Oke, O.; Ferguson, M. J.; McDonald, R.; Cowie, M. *Organometallics* **2005**, *24*, 4393. (c) Torkelson, J. R.; Antwi-Nsiah, F. H.; McDonald, R.; Cowie, M.; Pruis, J. G.; Jalkanen, K. J.; DeKock, R. L. *J. Am. Chem. Soc.* **1999**, *121*, 3666.

(12) Frisch, M. J.; Trucks, G. W.; Schlegel, H. B.; Scuseria, G. E.; Robb, M. A.; Cheeseman, J. R.; Montgomery, J. A., Jr.; Vreven, T.; Kudin, K. N.; Burant, J. C.; Millam, J. M.; Iyengar, S. S.; Tomasi, J.; Barone, V.; Mennucci, B.; Cossi, M.; Scalmani, G.; Rega, N.; Petersson, G. A.; Nakatsuji, H.; Hada, M.; Ehara, M.; Toyota, K.; Fukuda, R.; Hasegawa, J.; Ishida, M.; Nakajima, T.; Honda, Y.; Kitao, O.; Nakai, H.; Klene, M.; Li, X.; Knox, J. E.; Hratchian, H. P.; Cross, J. B.; Bakken, V.; Adamo, C.; Jaramillo, J.; Gomperts, R.; Stratmann, R. E.; Yazyev, O.; Austin, A. J.; Cammi, R.; Pomelli, C.; Ochterski, J. W.; Ayala, P. Y.; Morokuma, K.; Voth, G. A.; Salvador, P.; Dannenberg, J. J.; Zakrzewski, V. G.; Dapprich, S.; Daniels, A. D.; Strain, M. C.; Farkas, O.; Malick, D. K.; Rabuck, A. D.; Raghavachari, K.; Foresman, J. B.; Ortiz, J. V.; Cui, Q.; Baboul, A. G.; Clifford, S.; Cioslowski, J.; Stefanov, B. B.; Liu, G.; Liashenko, A.; Piskorz, P.; Komaromi, I.; Martin, R. L.; Fox, D. J.; Keith, T.; Al-Laham, M. A.; Peng, C. Y.; Nanayakkara, A.; Challacombe, M.; Gill, P. M. W.; Johnson, B.; Chen, W.; Wong, M. W.; Gonzalez, C.; Pople, J. A. *Gaussian 03*, Revision E.01; Gaussian, Inc.: Wallingford, CT, 2004.

(13) (a) Ernzerhof, M.; Scuseria, G. E. *J. Chem. Phys.* **1999**, *110*, 5029. (b) Ernzerhof, M.; Perdew, J. P.; Burke, K. *Int. J. Quantum Chem.* **1997**, *64*, 285.

(14) (a) Stratmann, R. E.; Scuseria, G. E.; Frisch, M. J. *J. Chem. Phys.* **1998**, *109*, 8218. (b) Bauernschmitt, R.; Ahlrichs, R. *Chem. Phys. Lett.* **1996**, *256*, 454. (c) Casida, M. E.; Jamorski, C.; Casida, K. C.; Salahub, D. R. *J. Chem. Phys.* **1998**, *108*, 4439.

(15) (a) Barone, V.; Cossi, M. *J. Phys. Chem. A* **1998**, *102*, 1995. (b) Cossi, M.; Rega, N.; Scalmani, G.; Barone, V. *J. Comput. Chem.* **2003**, *24*, 669.

(16) Andrae, D.; Häussermann, U.; Dolg, M.; Stoll, H.; Preuss, H. *Theor. Chim. Acta* **1990**, *77*, 123.

(17) (a) Hehre, W. J.; Ditchfield, R.; Pople, J. A. *J. Chem. Phys.* **1972**, *56*, 2257. (b) Hariharan, P. C.; Pople, J. A. *Theor. Chim. Acta* **1973**, *28*, 213. (c) Francl, M. M.; Pietro, W. J.; Hehre, W. J.; Binkley, J. S.; Gordon, M. S.; Defrees, D. J.; Pople, J. A. *J. Chem. Phys.* **1982**, *77*, 3654.

(18) Ehlers, A. W.; Böhme, M.; Dapprich, S.; Gobbi, A.; Höllwarth, A.; Jonas, V.; Köhler, K. F.; Stegmann, R.; Veldkamp, A.; Frenking, G. *Chem. Phys. Lett.* **1993**, *208*, 111.

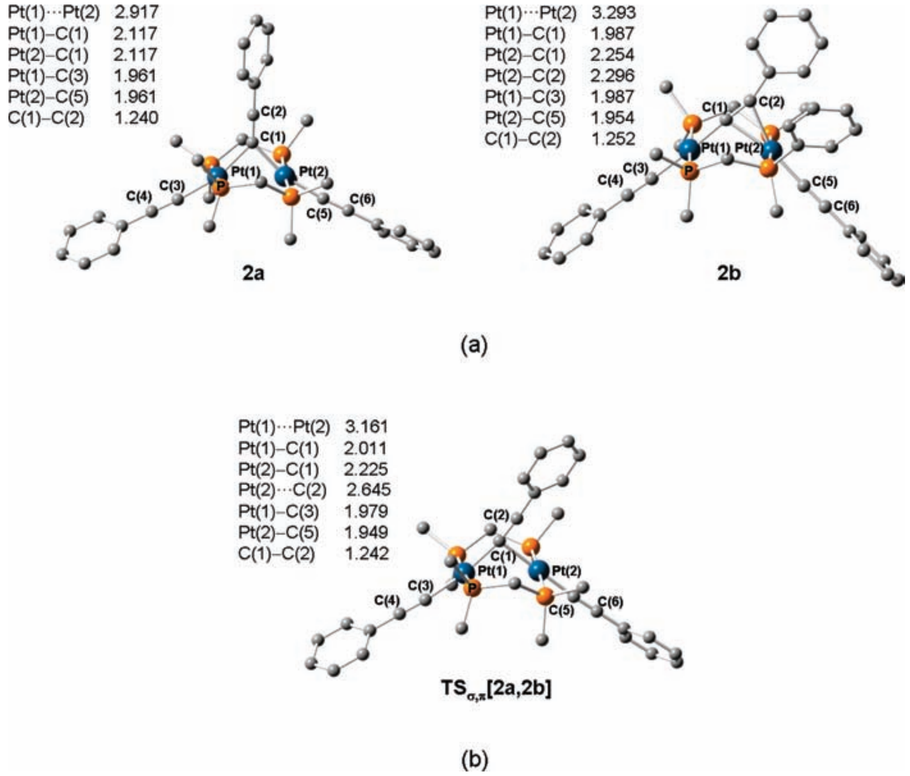

Figure 1. PBE0 optimized structures for (a) **2a** and **2b**, and (b) the transition state **TS$_{\sigma,\pi}$[2a,2b]** with selected bond distances (Å). For clarity, all hydrogen atoms and the phenyl rings on the dppm ligands with the exception of the *ipso* carbon atom are omitted.

functions for the P (ζ = 0.550) and alkynyl C atoms (ζ = 0.800)] were added.[17b,c] Unless mentioned otherwise, all the geometry optimizations were performed without any symmetry constraint. All DFT and TDDFT calculations were performed with a larger grid size (99590).

Results and Discussion

Ground-State Geometry. Geometry optimizations for complexes **1**–**5** (Scheme 2) in the symmetrical (**1a**–**5a**) and unsymmetrical forms (**1b**–**5b**) with the boat-structure conformation have been performed. Both complexes **5** and **6** have alkoxyphenyl substituents attached to the C≡C units. Only **5** was studied in detail. Both structural forms are found to be at a minimum in the potential energy surface. The optimized structures of the two forms in **2** with selected structural parameters are shown in Figure 1a, and the structural parameters for all the complexes are listed in the Supporting Information, Table S1. A discussion of the optimized structures for the two forms in **1**–**5** is given in the Supporting Information.

It is interesting to note that the Pt···Pt distance in the symmetrical form (2.917–2.948 Å) is significantly shorter than that in the unsymmetrical form (3.291–3.320 Å), indicating that the Pt···Pt distance is strongly dependent on the binding mode of the alkynyl ligands. The result is indeed in agreement with a shorter Pt···Pt distance found in the X-ray crystal structure of $[Pt_2(\mu\text{-dppm})_2(\mu\text{-C}{\equiv}CC_6H_4{}^n\text{Bu-}p)(C{\equiv}CC_6H_4{}^n\text{Bu-}p)_2]^+$ (2.903 Å) than that in **2** (3.236 Å), which is in the symmetrical and unsymmetrical forms, respectively. The shorter Pt···Pt distance found in the symmetrical form could be explained as follows. In the unsymmetrical form, the alkynyl C≡CR ligand functions as a four-electron donor to the two metals, whereas it is a two-electron donor ligand in the symmetrical form. The shorter Pt···Pt distance in the latter form is due to the presence of the electron-deficient three-center-two-electron bond involving the two metal centers and the alkynyl carbon atom. The influence in the binding mode of the alkynyl ligand on the nature of the metal–metal bonding in the A-frame complex has also been mentioned previously.[4c]

For all the complexes, the symmetrical form is calculated to be slightly lower in energy than the unsymmetrical form, in which the energy difference is in the range of 0.6–2.2 kcal mol^{-1}. The relatively small energy difference may account for the observation of the symmetrical and unsymmetrical forms in $[Pt_2(\mu\text{-dppm})_2(\mu\text{-C}{\equiv}CC_6H_4{}^n\text{Bu-}p)(C{\equiv}CC_6H_4{}^n\text{Bu-}p)_2]^+$ and **2** in the X-ray crystal structure, respectively.

Frontier Molecular Orbitals. To have a better insight into the nature of the transitions in the low-energy absorption band for the A-frame complexes, frontier molecular orbitals calculated for these complexes in the two forms have been examined. Figure 2 shows the spatial plots of selected TDDFT/CPCM frontier orbitals calculated for **2** in its two structural forms, and the percentage contribution of the selected molecular orbitals (MOs) for the symmetrical and unsymmetrical forms in all the complexes is listed in Supporting Information, Tables S2 and S3, respectively. Here, we use out-of-plane and in-plane π (or π*) orbitals to distinguish the two C≡C π bonding (or π* antibonding) orbitals in the C≡CAr ligand. The out-of-plane π or π* orbital is perpendicular to the plane of the aryl ring while the in-plane π or π* orbital is coplanar with the plane. For the symmetrical forms of the aryl-substituted alkynyl complexes **2a**–**5a**, the highest occupied molecular orbital (HOMO) of each is the linear combination of the out-of-plane π orbitals of the three alkynyl ligands mixed with the metal−metal dσ* antibonding orbital. It is noted that the M−C orbital overlap in the HOMO is antibonding in character. On the other hand, the lowest unoccupied molecular orbital (LUMO) of each is mainly the out-of-plane π* orbital of the bridging alkynyl ligand mixed in a bonding fashion with an out-of-phase combination of the two metal−ligand antibonding orbitals (see Figure 2a). It is worth mentioning that the LUMO+1 is the metal−metal pσ bonding orbital, with the P−C σ* orbitals of the dppm ligands contributing in a bonding fashion. For the unsymmetrical forms in **2b**−**5b**, the HOMO of each is the antibonding combination of the out-of plane π orbitals of the two terminal alkynyl ligands mixed in an antibonding fashion with the metal−metal dσ* antibonding orbital. Interestingly, unlike the LUMO in the symmetrical form, the LUMO in the unsymmetrical form is the metal−metal pσ bonding orbital mixed in a bonding fashion with the in-plane π* orbital of the bridging alkynyl ligand (Figure 2b). The stabilization of the metal−metal pσ bonding orbital in the unsymmetrical form is due to the right symmetry to positively overlap with the in-plane π* orbital of the bridging alkynyl ligand. On the other hand, the out-of-plane π* orbital of the bridging alkynyl ligand in the unsymmetrical form becomes higher-lying in energy, as it does not have the right symmetry to positively overlap with the out-of-phase combination of the metal−ligand antibonding orbitals. For the two structural forms of the *t*-butyl-substituted alkynyl complex, the molecular orbitals are similar to those discussed above in the aryl-substituted alkynyl complexes and will not be discussed further here.

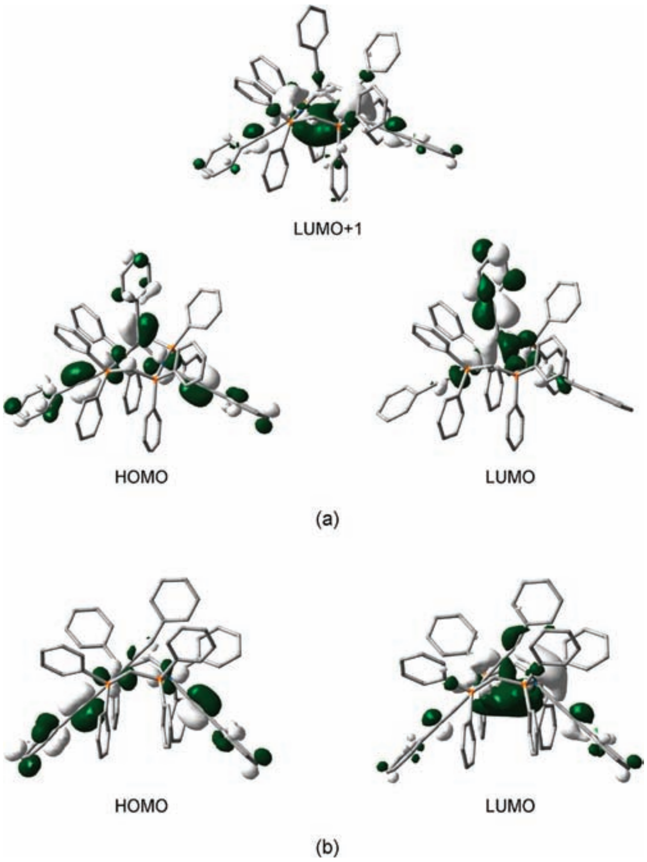

Figure 2. Spatial plots (isovalue = 0.03) of selected frontier molecular orbitals of the (a) symmetrical and (b) unsymmetrical forms in **2**.

The energy level diagrams of the selected frontier orbitals of the two forms in **1**−**5** are shown in the Supporting Information, Figure S1 to illustrate the effect on the orbital energies of the substituent R attached to the alkynyl ligand. For the two structural forms in **1**−**5**, the energies of the HOMO and LUMO are found to increase and decrease, respectively, from R = ^{t}Bu to R = Ph and to R = C_6H_4Ph-*p* because of the increase in the π-conjugation of the alkynyl ligand.

Nature of the Absorption and Emission. Table 1 lists the singlet−singlet transitions of the two forms in **1**−**5**. For the symmetrical form, the lowest-lying singlet−singlet transition computed at 401 and 438−460 nm for **1a** and **2a**−**5a**, respectively, is composed of HOMO → LUMO excitation. On the basis of the topology of the molecular orbitals, the transition can be assigned as admixture of an interligand $\pi \rightarrow \pi^*$ transition from the terminal alkynyl ligands to the bridging alkynyl ligand and the MMLCT [dσ*(Pt_2) → π*(bridging alkynyl)] transition. The second lowest-lying singlet−singlet transition is computed to be more intense for the *t*-butyl-substituted **1a** (370 nm) and the aryl-substituted **2a**−**5a** (401−418 nm) relative to the first singlet−singlet transition. This transition is mainly

Table 1. Selected Singlet−Singlet Transitions of the Symmetrical (**1a**−**5a**) and Unsymmetrical Forms (**1b**−**5b**) Computed by TDDFT/CPCM Using CH_3CN as the Solvent

complex	transition	orbital involved[a]	transition coefficient	f^b	vertical excitation wavelength (nm)
1a	$S_0 \rightarrow S_1$	H → L	0.67	0.037	401
	$S_0 \rightarrow S_2$	H → L+1	0.68	0.198	370
1b	$S_0 \rightarrow S_1$	H → L	0.67	0.277	367
2a	$S_0 \rightarrow S_1$	H → L	0.66	0.223	438
	$S_0 \rightarrow S_2$	H → L+1	0.68	0.420	401
2b	$S_0 \rightarrow S_1$	H → L	0.67	0.547	397
3a	$S_0 \rightarrow S_1$	H → L	0.67	0.475	460
	$S_0 \rightarrow S_2$	H → L+1	0.68	0.727	412
3b	$S_0 \rightarrow S_1$	H → L	0.67	0.809	412
4a	$S_0 \rightarrow S_1$	H → L	0.67	0.264	447
	$S_0 \rightarrow S_2$	H → L+1	0.68	0.463	409
4b	$S_0 \rightarrow S_1$	H → L	0.67	0.592	404
5a	$S_0 \rightarrow S_1$	H → L	0.67	0.278	459
	$S_0 \rightarrow S_2$	H → L+1	0.68	0.457	418
5b	$S_0 \rightarrow S_1$	H → L	0.67	0.579	416

[a] The orbitals involved in the major excitation (H = HOMO and L = LUMO). [b] Oscillator strengths.

Table 2. Selected Singlet−Triplet Transitions[a] of the Symmetrical (**1a**−**5a**) and Unsymmetrical Forms (**1b**−**5b**) Computed by TDDFT/CPCM Using CH_3CN as the Solvent

complex	transition	orbital involved[b]	transition coefficient	vertical excitation wavelength (nm)
1a	$S_0 \rightarrow T_1$	H → L	0.69	476
	$S_0 \rightarrow T_2$	H → L+1	0.69	404
1b	$S_0 \rightarrow T_1$	H → L	0.70	416
2a	$S_0 \rightarrow T_1$	H → L	0.69	557
	$S_0 \rightarrow T_2$	H → L+1	0.62	462
2b	$S_0 \rightarrow T_1$	H → L	0.64	475
3a	$S_0 \rightarrow T_1$	H → L	0.68	586
	$S_0 \rightarrow T_2$	H → L+1	0.57	487
3b	$S_0 \rightarrow T_1$	H → L	0.61	499
4a	$S_0 \rightarrow T_1$	H → L	0.69	565
	$S_0 \rightarrow T_2$	H → L+1	0.62	469
4b	$S_0 \rightarrow T_1$	H → L	0.64	481
5a	$S_0 \rightarrow T_1$	H → L	0.68	576
	$S_0 \rightarrow T_2$	H → L+1	0.63	476
5b	$S_0 \rightarrow T_1$	H → L	0.64	490

[a] The oscillator strengths for all the singlet−triplet transitions are zero. [b] The orbitals involved in the major excitation (H = HOMO and L = LUMO).

contributed to the excitation from the HOMO to the LUMO+1 and can be assigned as an admixture of a ligand-to-ligand charge-transfer (LLCT) [π(alkynyl) → σ*(dppm)] transition and a metal-centered MC [dσ*(Pt_2) → pσ(Pt_2)] transition. For the unsymmetrical form, the first singlet−singlet transition with significant oscillator strength composing of HOMO → LUMO excitation can be also assigned as an admixture of the LLCT [π(alkynyl) → σ*(dppm)]/MC [dσ*(Pt_2) → pσ(Pt_2)] transition. The transitions are computed at 367 and 397−416 nm for **1b** and **2b**−**5b**, respectively, which are roughly the same as the calculated LLCT [π(alkynyl) → σ*(dppm)]/MC [dσ*(Pt_2) → pσ(Pt_2)] transition in the symmetrical forms.

Supporting Information, Figure S2 shows the electronic absorption spectrum of **2** in acetonitrile.[9a] Complex **2** was found to exhibit a low-energy band centered at about 393 nm with a shoulder at about 450 nm. Similar findings have also been observed for the *t*-butyl substituted alkynyl complex **1** and aryl-substituted alkynyl complexes **3**−**5**, in which the low-energy band is centered at about 391 nm with a shoulder at about 410 nm and at about 394−408 nm with a shoulder at about 436−450 nm in the electronic absorption spectra of **1** and **3**−**5**, respectively.[9b] On the basis of the TDDFT/CPCM calculations of the two forms, the low-energy band centered at about 391 and 393−408 nm was due to LLCT [π(alkynyl) → σ*(dppm)]/MC [dσ*(Pt_2) → pσ(Pt_2)] transitions ($S_0 \rightarrow S_2$ transition in the symmetrical form and $S_0 \rightarrow S_1$ transition in the unsymmetrical form), while the shoulder at about 410 and 436−450 nm is due to the interligand π(terminal alkynyls) → π*(bridging alkynyl) transition mixed with the MMLCT [dσ*(Pt_2) → π*(bridging alkynyl)] transition. It is interesting to note that this transition is only present in the symmetrical form. The two types of transitions in **1** (367−370 and 401 nm) are computed to be at higher energy than that of **2**−**5** (397−418 and 438−460 nm), which are in agreement with the trend observed in the experiment.

Previous studies showed that the luminescence lifetimes of complexes **1**−**5** are in the microsecond range, indicating that the emission originates from excited states of triplet parentage. Table 2 lists the singlet−triplet transitions in **1**−**5**, in which the calculated transitions follow the same order as the singlet−singlet transitions. The lowest-energy transition among the two structural forms is still the interligand π(terminal alkynyls) → π*(bridging alkynyl)/MMLCT [dσ*(Pt_2) → π*(bridging alkynyl)] transition (476−586 nm). The transition wavelength of the interligand π(terminal alkynyls) → π*(bridging alkynyl)/MMLCT [dσ*(Pt_2) → π*(bridging alkynyl)] triplet excited state is computed in the order of **3** (586 nm) < **5** (576 nm) < **4** (565 nm) < **2** (557 nm) < **1** (476 nm), which is consistent with the trend observed in the emission spectra (CH_3CN at 298 K): **3** (640 nm) < **5** (630 nm) < **4** (620 nm) < **2** (614 nm) < **1** (500 nm).

To determine the nature of the distortion in the lowest-lying triplet excited state, a geometry optimization was performed for the lowest-lying excited state in the symmetrical form **2a** starting from the ground-state structure by using the unrestricted Kohn−Sham approach (UPBE0). Supporting Information, Figure S3 shows the spatial plot of the lower and higher-energy singly occupied molecular orbitals (SOMOs), which are similar to the respective HOMO and LUMO in the optimized ground-state geometry of **2a**. Compared with the ground-state structure of **2a**, in the interligand π(terminal alkynyls) → π*(bridging alkynyl)/MMLCT [dσ*(Pt_2) → π*(bridging alkynyl)] triplet excited state, the distortion is found to mainly occur along the Pt_2-bridging alkynyl ligand units.[19] Optimization of the lowest-lying triplet state for the unsymmetrical form **2b** has been also performed. However, starting from the ground-state optimized structure of **2b**, optimization with an initial guess for the [HOMO → LUMO] excited state leads to a geometry which is the same as the interligand π(terminal alkynyls) → π*(bridging alkynyl)/MMLCT [dσ*(Pt_2) → π*(bridging alkynyl)] triplet excited state of **2a**. On the basis of the calculation, the emission of the complexes originates from the triplet interligand π(terminal alkynyls) → π*(bridging alkynyl)/MMLCT [dσ*(Pt_2) → π*(bridging alkynyl)] excited state. The emission maximum of **2**, estimated from the difference in the solvent-corrected singlet and triplet energies at the optimized triplet excited-state geometry (ΔSCF method), is calculated to be 726 nm (see Supporting Information, Figure S4).[20] Although the calculated emission maximum

---

[19] The two Pt−C_α and C_β−C(phenyl) bond distances of the bridging ligand are shortened by 0.058 and 0.038 Å, respectively, while the C≡C and Pt(1)···Pt(2) distances are lengthened by 0.044 and 0.041 Å, respectively. All the Pt−P and Pt−C_α bond distances of the terminal ligands are slightly lengthened by 0.012−0.013 and 0.021 Å, respectively.

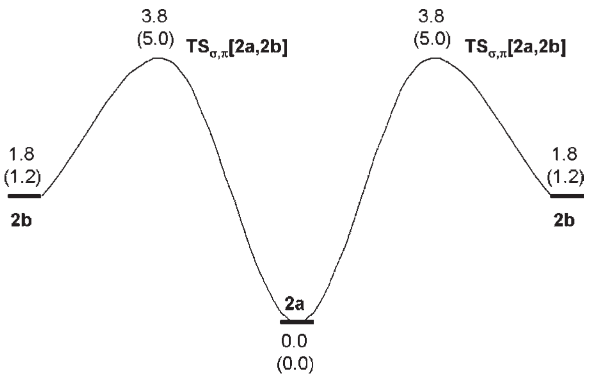

Figure 3. Potential energy profiles for the σ,π-alkynyl exchange process in **2** with the relative reaction energies and relative free energies in parentheses (kcal mol^{-1}).

is red-shifted by 0.31 eV compared with the one observed in the emission spectrum, similar underestimation of the emission energies can also be found in previous studies using the ΔSCF approach.[21]

Fluxional Processes. As mentioned in the introduction, three fluxional processes have been proposed based on previous NMR studies (Scheme 3). To have a better understanding of the fluxional behavior of the A-frame complexes, complex **2** has been chosen to study the details of the fluxional processes. For comparison, the fluxional process of **1** has also been investigated. In the following discussion, the electronic energy of the stationary points in **1** and **2** are described relative to the corresponding symmetrical boat form with the relative free energies shown in parentheses.

(a) ***σ,π*-Alkynyl Exchange.** Calculations have been performed to study the σ,π-alkynyl exchange process shown in Scheme 3a. As both the unsymmetrical and symmetrical forms are at the minima on the potential energy surface, one would expect the σ,π-alkynyl exchange to occur in a stepwise manner, which includes the transformation of the unsymmetrical to the symmetrical form, followed by the transformation of the symmetrical form back to the unsymmetrical form, with the latter step the exact reverse of the former. The transition state (**TS**$_{\sigma,\pi}$**[2a,2b]**) connecting **2b** and **2a** is calculated to be 1.9 (3.9) kcal mol^{-1} higher in energy than **2b**. In the transition state, the C(2) atom is further away from the Pt(2) metal center, but the C(1) atom is found to be slightly closer to the Pt(2) center, in which the Pt(2)−C(2) and Pt(2)−C(1) distances are lengthened and shortened by 0.349 Å and 0.029 Å, respectively (see Figure 1b). In addition, the Pt(1)$\cdots$Pt(2) distance is shortened by 0.132 Å in the transition state, when compared with **2b**. Figure 3 shows the potential energy profile for the σ,π-alkynyl exchange process. The activation barrier for the σ,π-alkynyl exchange process in **2** can be considered as 3.8 (5.0) kcal mol^{-1}, which is the barrier for the transformation of the symmetrical to the unsymmetrical form. For **1**, the unsymmetrical form and the transition state for connecting the two forms are calculated to be 0.6 (1.7) and 1.4 (3.1) kcal mol^{-1} higher in energy than the symmetrical form, respectively. The small barrier calculated in **1** and **2** indicates that the σ,π-alkynyl exchange is facile and is consistent with the experimental observation, in which only two sets of resonances were observed for the alkynyl groups in **1**, **5**, and **6** even at −40 °C.

(b) Ring-Flipping and Bridging-to-Terminal Alkynyl Exchange Processes. For the study of the ring-flipping and bridging-to-terminal alkynyl exchange processes, we would only confine our study to include those species derived from the bridging alkynyl ligand that binds in a symmetrical manner. As mentioned in the Introduction, both ring-flipping and bridging-to-terminal alkynyl exchange processes will result in the formation of the inverted-boat structure. Figure 4 shows the optimized structures of the boat **2a** and the inverted-boat (**2a′**) forms. The boat structure, which is commonly found in the A-frame system, is calculated to be 11.7 (13.4) kcal mol^{-1} lower in energy than the inverted-boat structure, indicating that the formation of the inverted-boat structure is thermodynamically unfavorable. The relatively unstable inverted-boat structure is due to the steric repulsion between the phenyl rings on the dppm ligands and the alkynyl ligands on the equatorial plane.[4f] As depicted in Figure 1a, the phenyl rings of the dppm ligands are staggered with respect to the equatorial ligands in **2a**. However, the phenyl rings come closer to the equatorial alkynyl ligands in the inverted-boat structure, in which the average absolute dihedral angles C(phenyls toward to the apex)−P−Pt−C(bridging alkynyl) and C(phenyls away from the apex)−P−Pt−C(terminal alkynyl) decrease from **2a** (91.8 and 51.3°) to **2a′** (63.6 and 22.2°), resulting in unfavorable contacts. Further support for the steric argument is provided by the DFT calculations using the same level of theory and basis set on simpler models for the boat and inverted boat structures, in which the phenyl rings attached to the P atoms were replaced by hydrogen atoms. The energy difference between the two structural forms with the simpler models is reduced to 0.5 kcal mol^{-1}.

There are two possible mechanisms for the ring-flipping process. One is the concerted pathway, in which two methylene carbon atoms of the dppm ligands flip simultaneously away from the apical position via the formation of the planar transition state ($C_2P_4Pt_2$ atom being on the same plane) (Scheme 4). The other is the stepwise pathway, in which one of the methylene carbon atoms is flipped at a time via the formation of the chair structure as an intermediate.

For the stepwise pathway, the chair structure (**2a″**) is calculated to be 5.5 (6.3) kcal mol^{-1} higher in energy than the boat structure **2a**. As depicted in Figure 4, in the chair structure, one methylene group is pointing way from and the other is toward the apical position, in which the interplanar angles between P(1)−Pt(1)−Pt(2)−P(3) and the P(1)−C(7)−P(3) planes as well as P(2)−Pt(1)−Pt(2)−P(4) and the P(2)−C(8)−P(4) planes are 30.9 and 43.5°, respectively. The transition states (**TS**$_{\text{flip}}$**[2a,2a″]** and **TS**$_{\text{flip}}$**[2a′,2a″]**) connecting **2a** and **2a″** as well as **2a″** and **2a′** have been found. As shown in Figure 4, the

---

(20) The calculated emission maximum was estimated from the differences between the triplet excited state and ground state energies obtained from single-point CPCM calculations (CH_3CN as a solvent) at the optimized triplet state geometry.

(21) (a) Ladouceur, S.; Fortin, D.; Zysman-Colman, E. *Inorg. Chem.* **2010**, *49*, 5625. (b) Salassa, L.; Garino, C.; Albertino, A.; Volpi, G.; Nervi, C.; Gobetto, R.; Hardcastle, K. I. *Organometallics* **2008**, *27*, 1427. (c) Lowry, M. S.; Hudson, W. R.; Pascal, R. A., Jr.; Bernhard, S. *J. Am. Chem. Soc.* **2004**, *126*, 14129.

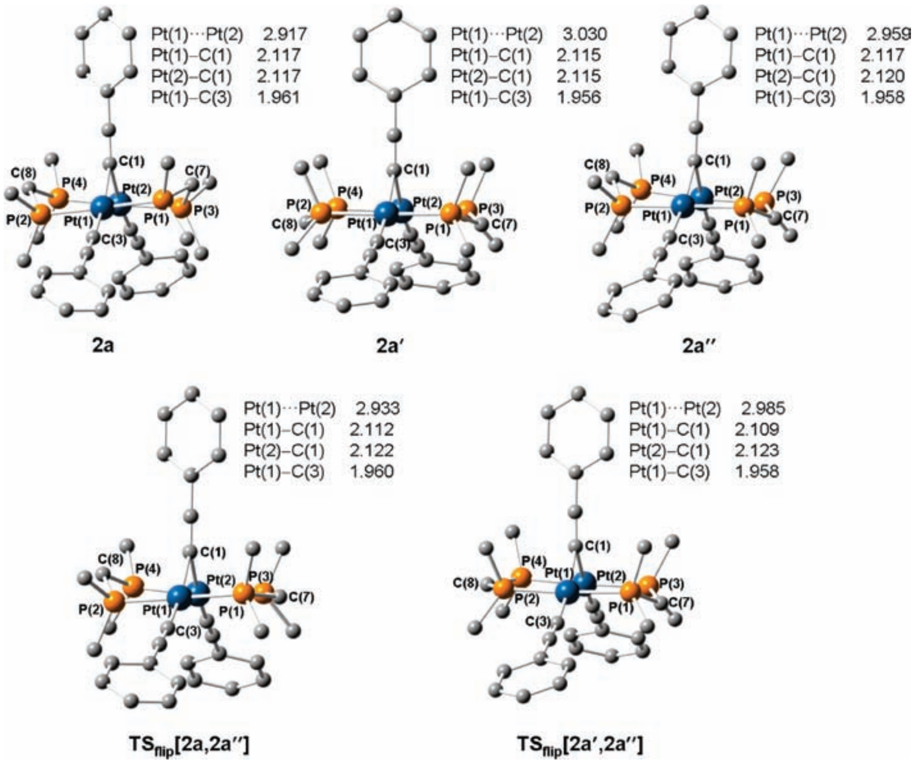

Figure 4. PBE0 optimized structures (side view) for the species involved in the ring-flipping process with selected bond distances (Å). For clarity, all hydrogen atoms and the phenyl rings on the dppm ligands with the exception of the *ipso* carbon are omitted.

methylene carbon C(7) and C(8) are lying more or less on the plane of the P(1)−Pt(1)−Pt(2)−P(3) and P(2)−Pt(1)−Pt(2)−P(4) in **TS$_{\mathbf{flip}}$[2a,2a″]** and **TS$_{\mathbf{flip}}$[2a′,2a″]**, respectively, in which the interplanar angles between P(1)−Pt(1)−Pt(2)−P(3) and P(1)−C(7)−P(3), and P(2)−Pt(1)−Pt(2)−P(4) and P(2)−C(8)−P(4) planes are 9.9 and 6.8°.

For the concerted pathway, our attempts to generate a planar transition state connecting the two boat structures failed. The optimization of the transition state corresponding to the concerted planar structure shown in Scheme 4 leads to a structure close to the chair form. On the basis of the calculated result, the ring-flipping process should be more likely via the stepwise pathway. The **TS$_{\mathbf{flip}}$[2a,2a″]** and **TS$_{\mathbf{flip}}$[2a′,2a″]** are calculated to be 1.1 (1.8) kcal mol^{-1} and 1.0 (2.3) kcal mol^{-1} higher in energy than the chair and inverted-boat forms, respectively, indicating that the activation barrier for the reverse reaction, that is, the conversion from the inverted-boat form to the boat form, should be very small.

The transition state for the bridging-to-terminal alkynyl exchange (**TS$_{\mathbf{bt}}$[2a,2a′]**) connecting the two boat structures, **2a** and **2a′**, was located, and it is calculated to be 19.8 (22.0) kcal mol^{-1} higher in energy than **2a**. In the transition state, the C(1) alkynyl ligand is moving away from the Pt(2) center while the C(3) alkynyl ligand is moving toward the Pt(2) center, in which the C(1)−Pt(1)−Pt(2) is increased from 46.5° to 92.1° and the C(3)−Pt(1)−Pt(2) angle is decreased from 149.2° to 77.1° upon going from the boat structure and to the transition state (Figure 5a). It is interesting to note that the Pt···Pt separation in the transition state is calculated to be 2.767 Å, indicating that the two platinum atoms are directly bonded to one another. In addition, different coordination can be observed for the two Pt centers in the transition state. The Pt(2) assumes a distorted square planar geometry, coordinating to the two *trans* P atoms [P(3) and P(4)] from the two dppm ligands, the alkynyl carbon atom C(5), and the Pt(1) atom, in which the P(3)−Pt(2)−P(4) and Pt(1)−Pt(2)−C(5) angles are 168.7 and 176.7°, respectively. However, the coordination geometry at the Pt(1) can be described as a distorted square pyramid [basal plane defined by two *trans* P atoms [P(1) and P(2)] and two *trans* alkynyl carbon atoms [C(1) and C(3)] with Pt(2) atom at the apex]. The shortening of the Pt−Pt distance in the transition state is predicted on the basis of electron counting. Without a metal−metal bond, one metal center has 16 valence electrons while the other has only 14 electrons. A dative bond alleviates the electron deficiency at the second metal. The bonding between the Pt(1) and Pt(2) atoms can be described as a Pt(II)→Pt(II) donor−acceptor interaction, which involves donation of electron density from the filled d_{z^2} orbital of the square-planar [Pt(l)P_2C_2] unit to a vacant acceptor orbital of the [Pt(2)P_2C]$^+$ unit. A similar bonding interaction was previously discussed in the dinuclear platinum complex, [Pt_2Me_3(μ-dppm)$_2$]$^+$.[22a] Donor−acceptor species were also proposed to be involved in the bridging-to-terminal ligand exchange process of other A-frame complexes.[22b]

Previous NMR study suggested that the equivalence of both the alkynyl ligands and the methylene protons may originate from the same fluxional process, and the $\Delta G^{\ddagger}$

---

[22] (a) Brown, M. P.; Cooper, S. J.; Frew, A. A.; Manojlović-Muir, Lj.; Muir, K. W.; Puddephatt, R. J.; Seddon, K. R.; Thomson, M. A. *Inorg. Chem.* **1981**, *20*, 1500. (b) Puddephatt, R. J.; Azam, K. A.; Hill, R. H.; Brown, M. P.; Nelson, C. D.; Moulding, R. P.; Seddon, K. R.; Grossel, M. C. *J. Am. Chem. Soc.* **1983**, *105*, 5642.

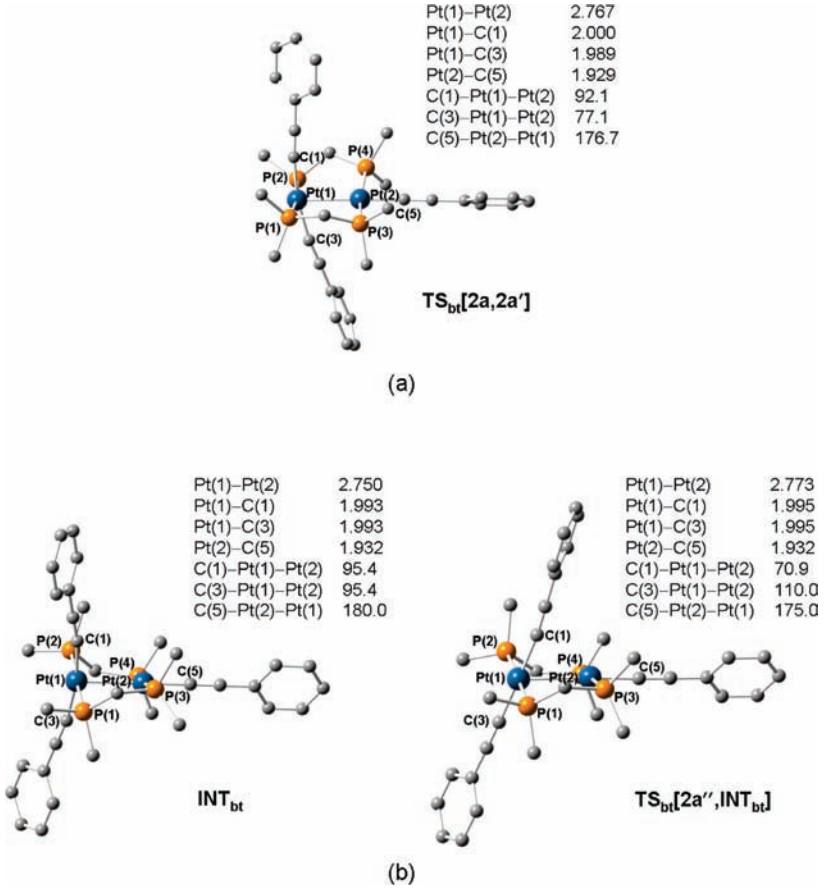

Figure 5. PBE0 optimized structures for the species involved in the bridging-to-terminal alkynyl exchange process, (a) the transition state $\mathbf{TS_{bt}[2a,2a']}$ and (b) the intermediate $\mathbf{INT_{bt}}$ and transition state $\mathbf{TS_{bt}[2a'',INT_{bt}]}$ with selected bond distances (Å) and angles (deg). For clarity, all hydrogen atoms and the phenyl rings on the dppm ligands with the exception of the *ipso* carbon are omitted.

value obtained is that measured for the bridging-to-terminal alkynyl exchange process. On the basis of the calculations, the fluxional process possibly involves the transformation from the boat structure to the inverted-boat structure via the bridging-to-terminal alkynyl exchange and followed by the retention of the boat structure through the ring-flipping process. Figure 6a shows the relative electronic energy profiles for the proposed fluxional process. As depicted, the bridging-to-terminal alkynyl exchange is the rate-determining process, in which the activation energy for the exchange process is calculated to be 19.8 (22.0) kcal mol^{-1}. Because of the instability of the inverted-boat structure, the retention of the boat structure can be achieved via the ring-flipping process. From the energy profile shown in Figure 6a, we can say that the experimentally measured $\Delta G^{\ddagger}$ is related to the bridging-to-terminal alkynyl exchange process. The calculated $\Delta G^{\ddagger}$ (22.0 kcal mol^{-1}) is higher than the experimental observed $\Delta G^{\ddagger}$ (15.5 kcal mol^{-1}).

Another possible pathway without proceeding via the formation of the inverted-boat structure is proposed (Scheme 5). It involves (i) the conversion from the boat form to the chair form via the ring-flipping process, (ii) the transformation from one chair form to another chair form through the bridging-to-terminal alkynyl exchange and followed by (iii) the conversion from the chair form back to the boat form via the ring-flipping process. Step (i) is the reverse process of the step (iii). The transition state connecting the boat structure and the chair structure via the ring-flipping process has been mentioned previously. For the transformation of the two chair forms

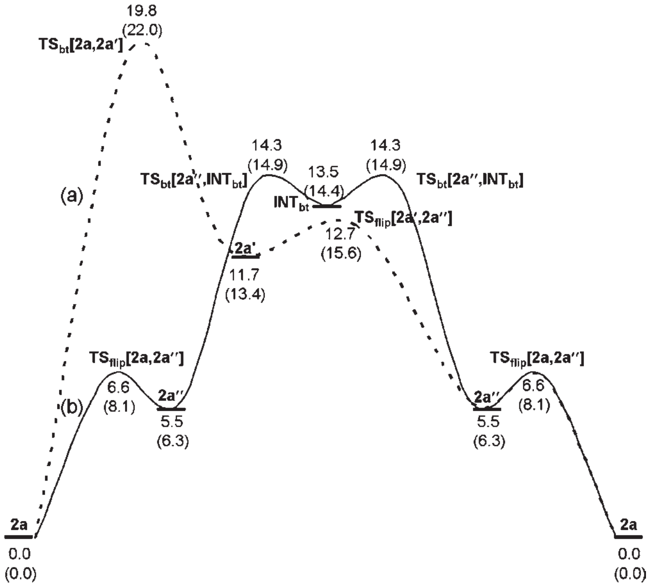

Figure 6. Potential energy profiles for the fluxionality involving the bridging-to-terminal alkynyl exchange and ring-flipping process in **2**, (a) via the inverted-boat structure and (b) without going through the inverted-boat structure. The relative reaction energies and relative free energies in parentheses are given in kcal mol^{-1}.

Scheme 5. Proposed Mechanism

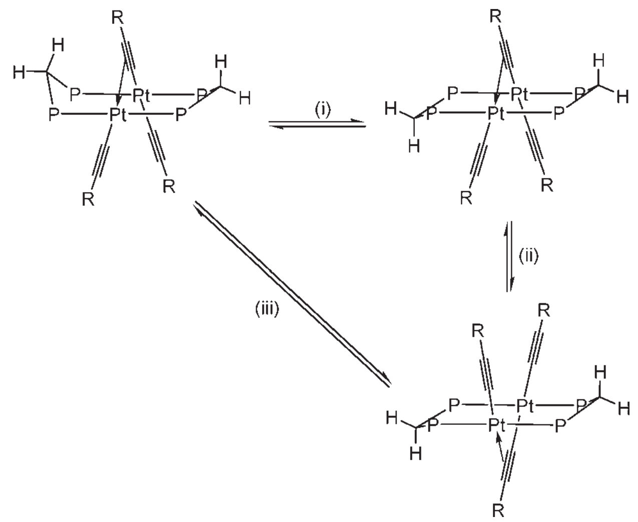

shown in step (ii), it is interesting to note that an intermediate with C_2 symmetry containing Pt(II)→Pt(II) donor–acceptor interaction ($\mathbf{INT_{bt}}$) is found (see Figure 5b). In contrast to the transformation of the two boat structures that proceeds via the bridging-to-terminal exchange, the Pt(II)→Pt(II) donor–acceptor species was found to be the transition state. The Pt–Pt distance is calculated to be 2.750 Å and both the C(1)–Pt(1)–Pt(2) and the C(3)–Pt(1)–Pt(2) angles are 95.4°. The transition state ($\mathbf{TS_{bt}[2a'', INT_{bt}]}$) connecting **2a**″ and the Pt(II)→Pt(II) donor–acceptor intermediate $\mathbf{INT_{bt}}$ is also shown in Figure 5b. A longer Pt–Pt distance (2.773 Å) is found in $\mathbf{TS_{bt}[2a'', INT_{bt}]}$ when compared with that in $\mathbf{INT_{bt}}$. The $\mathbf{TS_{bt}[2a'', INT_{bt}]}$ and $\mathbf{INT_{bt}}$ are calculated to be 14.3 (14.9) and 13.5 (14.4) kcal mol^{-1} higher in energy than **2a**, respectively. Figure 6b depicts the potential energy profile for the proposed mechanism shown in Scheme 5. As depicted, the bridging-to-terminal alkynyl exchange process is the rate-determining step. The calculated $\Delta G^{\ddagger}$ value of the overall reaction for **2** is 14.3 (14.9) kcal mol^{-1}, while that for **1** is 14.0 (16.3) kcal mol^{-1}, both of which are close to the experimentally observed $\Delta G^{\ddagger}$ for the A-frame alkynyl complexes (15.5 kcal mol^{-1}). The calculation demonstrates that the fluxional process via the inverted-boat structure is energetically less favorable.

Conclusion

DFT and TDDFT/CPCM calculations have been successfully applied to investigate the structure, the nature of the low-energy absorption and emission, and the mechanism for the fluxionality observed from the NMR study. The result shows that a significantly shorter Pt$\cdots$Pt distance is found in the symmetrical form than that in the unsymmetrical form. The shorter Pt$\cdots$Pt distance in the former could be explained by the presence of the electron-deficient three-center-two-electron bond involving the two metal centers and the alkynyl carbon atom. The TDDFT/CPCM calculation shows that the excited state involved in the lowest-energy absorption and emission consists of interligand π(terminal alkynyls) → π^*(bridging alkynyl)/MMLCT [dσ^*(Pt$_2$) → π^*(bridging alkynyl)] characters. In terms of the fluxional behaviors, a small activation barrier is computed for the σ,π-exchange process. The proposed mechanism for the fluxional process, which leads to the equivalence of the methylene and alkynyl signals, is shown in Scheme 5. The calculated $\Delta G^{\ddagger}$ for the overall fluxional process is in good agreement with the experimentally determined $\Delta G^{\ddagger}$.

Acknowledgment. V.W.-W.Y. acknowledges support from The University of Hong Kong under the Distinguished Research Achievement Award Scheme and the URC Strategic Research Theme on Molecular Materials. This work has been supported by the University Grants Committee Areas of Excellence Scheme (AoE/P-03/08). W.H.L. acknowledges support from the URC Seed Funding for Basic Research from The University of Hong Kong (200905159002). We also thank the Computer Center at The University of Hong Kong for providing the computational resources.

Supporting Information Available: Table S1 containing selected structural parameters for the optimized symmetrical (**1a**–**5a**) and unsymmetrical forms (**1b**–**5b**), Tables S2 and S3 containing the calculated percentage composition of the selected MOs, Figure S1 containing the orbital energy diagram, Figure S2 containing the electronic absorption spectrum of **2** in acetonitrile, Figure S3 containing spatial plots of the low-energy and higher-energy SOMOs in **2a**, Figure S4 containing the schematic energy diagram of the vertical excitation and emission wavelengths for **2**, and Cartesian coordinates for the optimized geometries. This material is available free of charge via the Internet at http://pubs.acs.org.